

Chapter 5

High-Q surface plasmon-polariton microcavity

5.1 Introduction

As the research presented in this thesis has shown, microcavities are ideal vehicles for studying light and matter interaction due to their resonant property, which allows individual photons to sample their environment thousands of times. Accurate loss characterization is possible through Q factor measurements, which can elucidate origins of loss if the measurements are performed while varying factors under study (e.g., presence of water).

This chapter explores the interaction of light and metal in surface plasmon polariton (SPP) microcavity resonators. The aim of this research effort is to accurately quantify metal loss for SPP waves traveling at the interface between glass and silver. The electric field components of SPP modes in the resonator are calculated by FEM simulation. Two types of plasmonic microcavity resonators are built and tested based on the microtoroid, and microdisk. Only dielectric resonances are observed in the microtoroid resonator, where the optical radiation is attenuated by a metal coating at the surface. However, a silver coated silica microdisk resonator is demonstrated with surface plasmon resonances. In fact, the plasmonic microdisk resonator has record Q for any plasmonic microresonator. Potential applications of a high quality plasmonic waveguide include on-chip, high-frequency communication and sensing.

5.1.1 Plasmonics

A plasmon is an oscillation of the free electron gas that resides in metals. Plasmons are easy to excite in metals because of the abundance of loosely bound, or free, electrons in the highest valence shell. These electrons physically respond to electric fields, either present in a crystal or from an external source. Obviously, light contains electric field components and can therefore modify the electron gas in a metal. In fact, photons incident on a metal conductor at a frequency less than the plasmon frequency will be reflected. But, if the optical frequency is higher than the plasmon frequency, then the light will be transmitted through the metal since the electrons cannot respond fast enough to screen the light. What if light could interact with a metal in a third manner, one not of reflection or transmission? Such a field exists, named surface plasmonics, and involves traveling

waves of electron oscillation in a metal.

5.1.2 Surface plasmon polaritons

Surface plasmons are electron oscillations that are confined to the interface of a metal and a dielectric, for example glass or air. Due to their high electric field components at the surface, surface plasmons are extremely sensitive to surface particles. Surface plasmons have gained significant attention for their high frequencies, as high as 100 THz. High bandwidth transmission lines could be created using surface plasmonics for on-chip computing.

A polariton can be described as a particle, one that results from strong coupling of electromagnetic waves (i.e., light) with electric dipoles (i.e., electron gas). If light is incident on a metal with a momentum matched to that of the SPP mode, then the optical wave can couple into a surface plasmon polariton wave traveling at the surface of the metal. Also, a SPP wave can couple out of the metal and thus reappear as light. This effect is demonstrated by fiber taper coupling of light into and out of a SPP resonator.

5.1.3 Plasmon resonator concept

Whereas optical micro- and nanocavities made of dielectric or semiconducting materials exhibit large Q factors as well as small diffraction-limited cavity mode volumes, their metallic counterparts (surface-plasmonic cavities [24, 25, 87, 26, 88, 89, 90, 91] have been optimized primarily for subwavelength-scale miniaturization and have given results well below the theoretically predicted performance limit—especially in terms of cavity loss—set by ohmic loss in the metal. This is believed to result from other loss contributions such as surface scattering, radiation, finite cavity mirror reflectance or a significant degree of field penetration into the metal. However, these seemingly distinct dielectric and plasmonic waveguiding principles can be combined in a single cavity by using mature optical microcavity technology such as that provided by disk [9, 92] or toroidal microcavities [10]. A surface-plasmonic whispering-gallery microcavity with a cavity plasmon-polariton loss rate close to the theoretical limit will be presented.

5.2 Microtoroid plasmonic resonator

The search for SPP resonances in a microcavity started with a gold coated ultra-high Q microtoroid. At first glance, the microtoroid appears to be better suited than the lower intrinsic optical Q microdisk due to the smoother surface finish formed by selective CO₂ laser reflow. However, near ideal Q SPP resonances will be observed in a silver coated microdisk, possibly due to better coating uniformity and absence of the thin chrome layer.

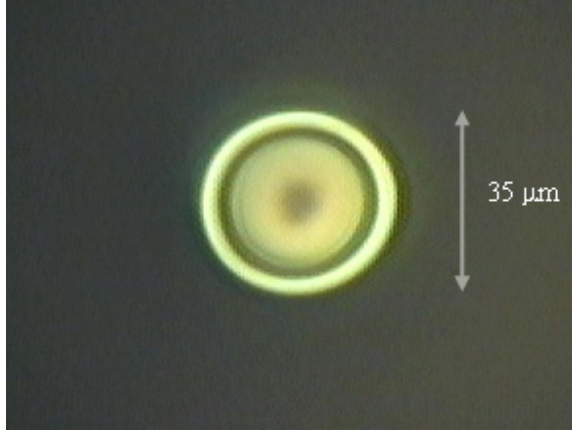


Figure 5.1. Microscope image of a silica microtoroid coated with 200 nm gold coating (top view)

5.2.1 Fabrication of metal coated microtoroid resonator

A small diameter ($D = 34 \mu\text{m}$) microtoroid is fabricated by lithography, etching, and laser reflow. First, a 10 nm layer of chromium is deposited by vacuum sputtering for adhesion. Next, a 200 nm layer of gold is sputtered onto the microtoroids. Gold was chosen because it has lower loss than most metals, except for silver. Figure 5.1 is a microscope image of the gold coated toroid.

5.2.2 Microtoroid resonator results

The gold coated microtoroid resonator is probed optically with a sub-micron diameter fiber taper. For best coupling to the dielectric modes observed in the gold coated toroid, the fiber taper is located underneath the toroid. In this position, the injected optical wave does not have to tunnel through the gold layer. The spectrum of the gold coated toroid resonator was measured using a single frequency tunable laser scanned from 1525 to 1570 nm. The taper transmission, showing the resonance locations, is recorded using a low-noise photodetector.

The resonator spectrum exhibits three resonances as shown in Figure 5.2, locations of propagating modes in the microtoroid. The three resonances are smooth, and appear to correspond to the same mode based on the identical resonance widths and free spectral range (FSR) of the modes. The critical coupled Quality factor is 390, and the FSR is 15 nm. For this toroid's diameter of $3 \mu\text{m}$, the FSR indicates an experimental effective cavity mode index (n_{eff}) of 1.45. The resonances observed in this gold coated microtoroid are confirmed to be lossy dielectric modes.

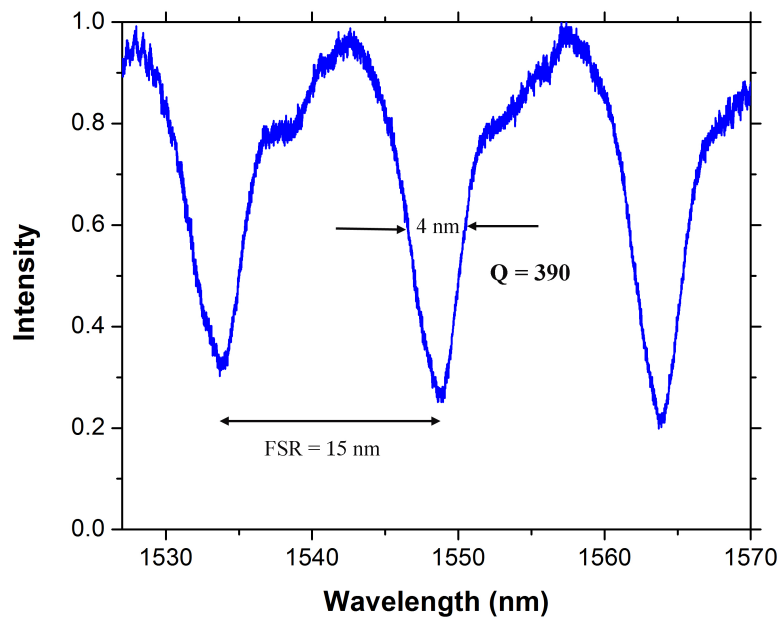


Figure 5.2. Plot of fiber taper transmission versus wavelength of coupling to a gold coated micro-toroid showing frequency spectrum of a lossy dielectric mode. Three resonances are shown, corresponding to the same longitudinal mode. The free-spectral range and resonance FWHM linewidth are marked. The resonance $Q = 390$, and $FSR = 15$ nm.

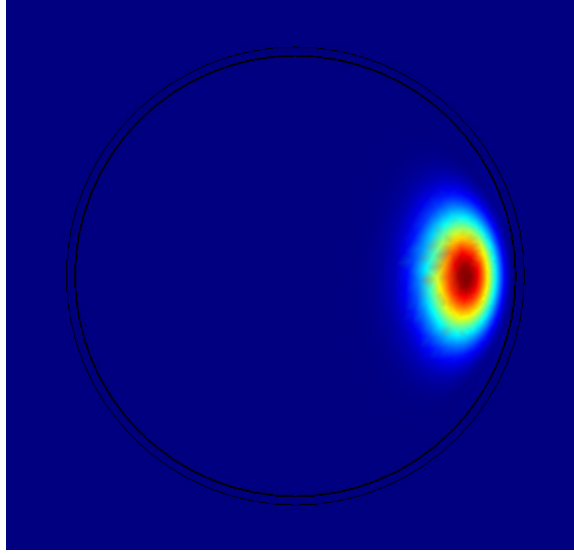


Figure 5.3. Plot of the dielectric cavity mode of a gold-coated microtoroid generated by FEM simulation. The innermost coating is 10 nm of chrome (not visible), and the outer coating is 150 nm of gold (visible).

Bumki Min developed a fully-vectorial finite element model of the silica microtoroid with the 10 nm chrome and the 150 nm gold layers. A cross-sectional image of the fundamental dielectric mode of metal coated microtoroid resonator is shown in Figure 5.3. The dielectric mode's power is confined inside the silica, and decays exponentially within the metal. FEM simulation of the mode for adjacent longitudinal mode numbers, m , determines the cavity mode effective index $n_{eff} = 1.45$, identical to experimental results. Therefore, the only resonances confirmed in the gold coated microtoroid cavity are lossy dielectric modes. One reason for the lack of SPP modes, which have lower Q than dielectric modes, may be non-conformal coating of the microtoroid due to its circular cross section. However, a collaboration between the author and Bumki Min successfully demonstrates a SPP microdisk resonator. The linear geometry of the microdisk bevel edge produces more uniform metal coating of the resonator.

5.3 Microdisk based plasmonic resonator

5.3.1 Plasmonic disk resonator fabrication

A plasmonic microdisk cavity structure is shown in Figure 5.4a. The plasmonic cavity is composed of a silica (silicon dioxide) disk microcavity coated with a thin layer of silver. Silica microdisk resonators are ideal templates for the study of surface-plasmonic whispering-gallery modes primarily because they routinely have optical Q factors greater than 10^6 . Using the wedge structure shown in Figure 5.4a, Q factors as high as 6×10^7 have been demonstrated [9].

The silica microdisks are fabricated by photolithography and a modified buffered oxide etching. During the wet etch, the photoresist is undercut and produces a bevelled silica edge, which provides conformal silver coating of the top surface of the microdisk. The bevel angle is determined by additional etching time and control of adhesion between the resist and silica layer. The silver coating is deposited on the template silica microdisks using a d.c. sputtering technique with a chamber argon pressure of 30 mtorr.

Two batches of samples (series 1 and 2) are prepared in this way to investigate the size-dependent characteristics of SPP microcavities. A scanning electron image of a silver-coated SPP microdisk resonator is shown in Figure 5.4b, and an expanded view of the edge of the disk resonator is shown in Figure 5.4c.

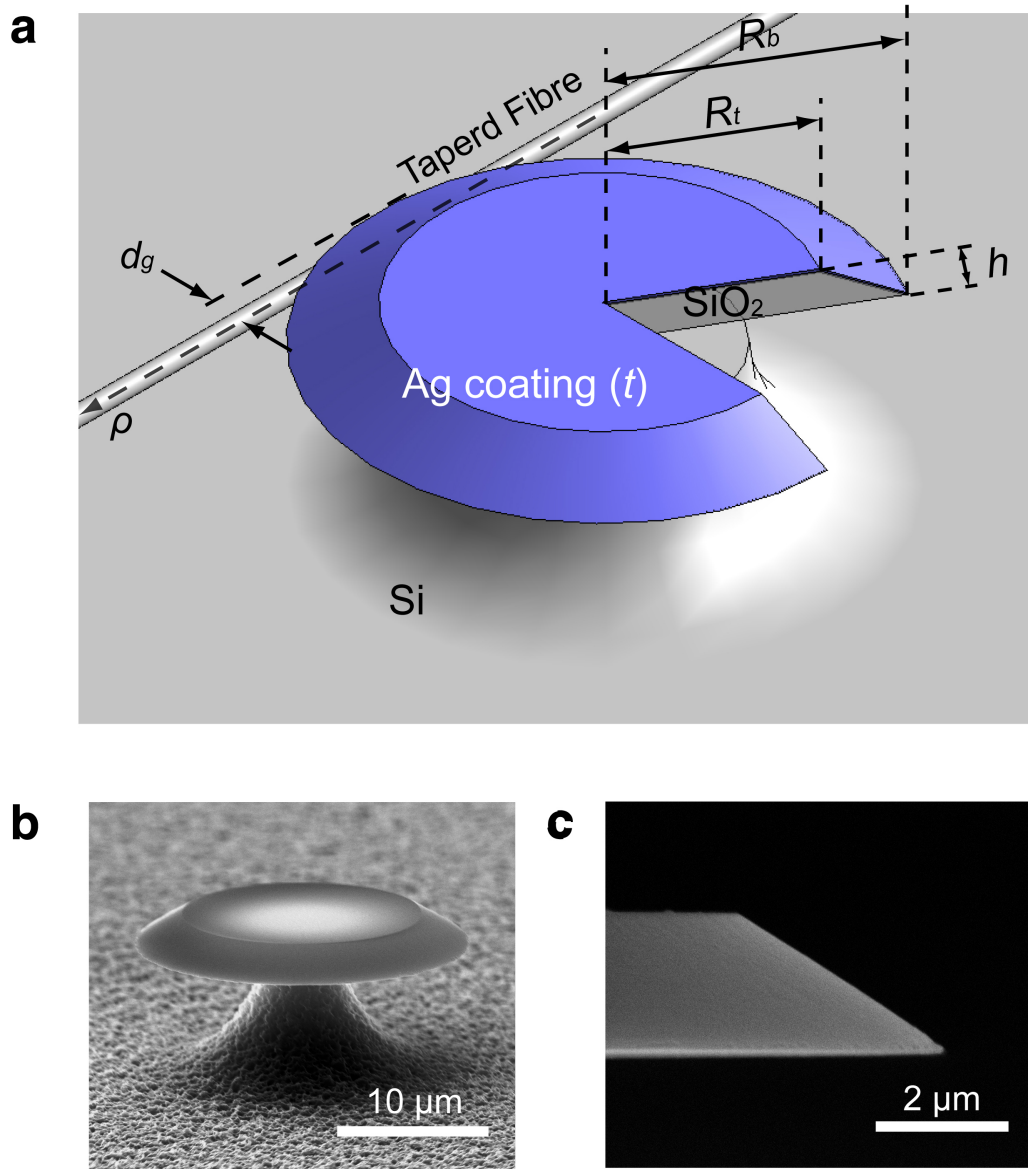


Figure 5.4. **a**, SPP microdisk resonator with a tapered optical fiber passing under its edge. The wedge-shaped disk edge is a by-product of isotropic buffered hydrofluoric acid etching of silica. A transverse cross-section of the cavity is shown for clarity. R_b —bottom radius; R_t —top radius; d —thickness of the silica disk resonator; t —thickness of the metal layer. The straight fiber waveguide axis is denoted by the coordinate ρ and the gap width, d_g , is defined as the horizontal distance from the dielectric cavity edge to the fiber axis. **b**, Scanning electron micrograph of a fabricated silver-coated SPP microdisk resonator ($R_b = 10.96 \mu\text{m}$, $R_t = 57.89 \mu\text{m}$, $d = 2 \mu\text{m}$, $t \approx 100 \text{ nm}$). **c**, Expanded view of the edge of the SPP microdisk resonator.

5.4 Finite-element model of SPP resonator

A full vectorial finite-element analysis was performed for the SPP microdisk resonators [11, 93], taking into account the effects of silver [94] and silica [95] material dispersion. The theoretical cavity mode dispersion diagram of an SPP microdisk resonator (Figure 5.5) shows the real part of the eigenfrequency, f , of the cavity modes as a function of an azimuthal mode number, m . The vacuum light line is defined by $f = \frac{mc}{2\pi R_b}$ with respect to the bottom radius, R_b , of the template silica disk microcavity, and the silica light line is similarly defined by $f = \frac{mc}{2\pi n_{silica}(f)R_b}$. Note that c is the speed of light and n_{silica} is the refractive index of silica. The eigenmodes of an SPP microcavity can be classified into two distinctive categories in terms of the cavity mode dispersion: (1) surface-plasmonic modes at the metal-dielectric interface and (2) optical dielectric modes due to the presence of a dielectric waveguiding channel. The dielectric modes are similar to those observed in the gold coated microtoroid.

In the insets of Figure 5.5, the fundamental SPP eigenmode, the second-order SPP eigenmode and the fundamental dielectric eigenmode are plotted for magnetic energy density $u_M = (1/2\mu_0)|\mathbf{B}(r, \phi, z)|^2$ (where μ_0 is the permeability of free space) using a false-color map (a conventional cylindrical coordinate system (r, ϕ, z) is used for the analysis). The SPP eigenmodes of an SPP microdisk resonator have electromagnetic energy-density profiles with a peak at the silica-metal interface in the transverse plane (constant ϕ). The SPP eigenmodes are identified as SPP $_{qm}$, where q is the plasmonic mode number ($\mathbf{H}(r, \phi, z) = \mathbf{H}_{\text{SPP}}^{qm}(r, z)e^{im\phi}$), and the optical dielectric eigenmodes are denoted by DE $_{hm}$, where h is the dielectric mode number ($\mathbf{H}(r, \phi, z) = \mathbf{H}_{\text{DE}}^{hm}(r, z)e^{im\phi}$). The plasmonic mode number is defined as the number of antinodes in $|\mathbf{H}_{\text{SPP}}^{qm}|$ along the silica-metal interface (excluding the vicinity of the sharp corner of the microcavity). Dispersion relations for the four lowest-order SPP eigenmodes ($q = 1, 2, 3, 4$) and the two lowest-order dielectric eigenmodes ($h = 1, 2$) are plotted in Figure 5.5. The mode numbers, $h = 1, 2, \dots$, of the dielectric eigenmodes DE $_{hm}$ are assigned in order from lowest to highest order dielectric eigenmode. Depending on the geometry and the mode number h , dielectric eigenmodes can possess certain degrees of plasmonic characteristics due to the presence of the metal-silica interface.

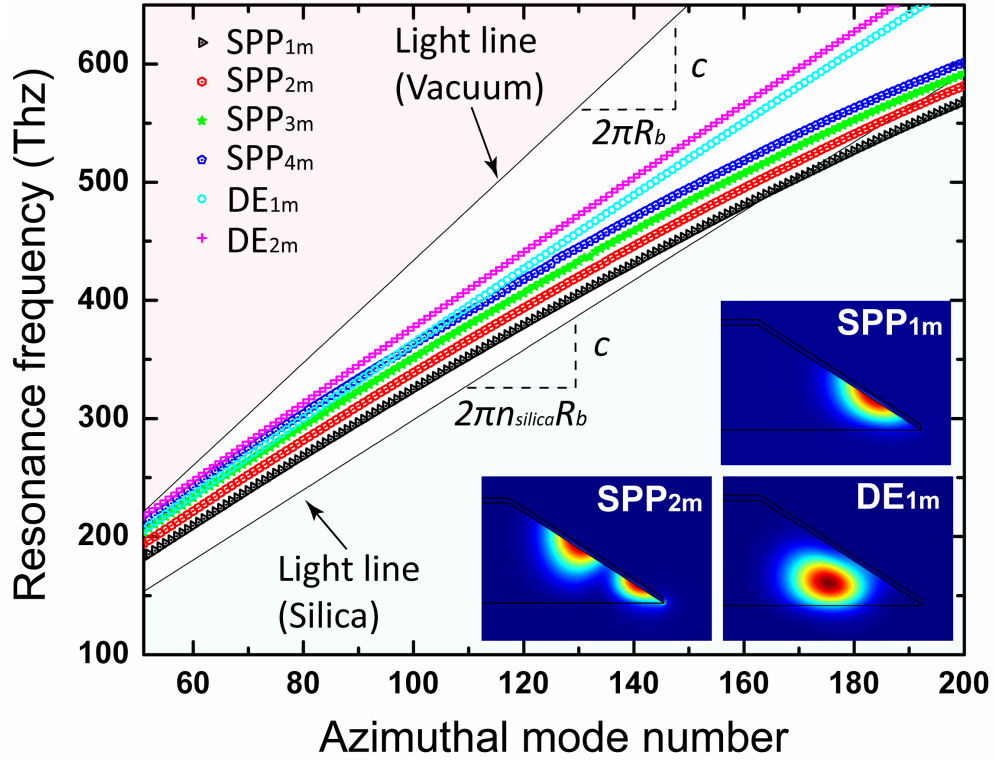


Figure 5.5. Cavity mode dispersion curves for an SPP microdisk resonator, calculated from finite-element eigenfrequency analysis. For this calculation, the thickness of the silver layer is 100 nm, and the bottom and top radii and the thickness of the template silica microdisk resonator were set to 11, 7.9, and 2 μ m, respectively. Light lines, corresponding to vacuum and silica, are given as two black lines (silica material dispersion has been taken into account). For clarity, only the four lowest-order SPP eigenmodes and the two lowest order dielectric eigenmodes are plotted. The first- and second-order SPP eigenmodes (SPP_{1m}, SPP_{2m}) and the fundamental dielectric eigenmode (DE_{1m}) are shown in the inset.

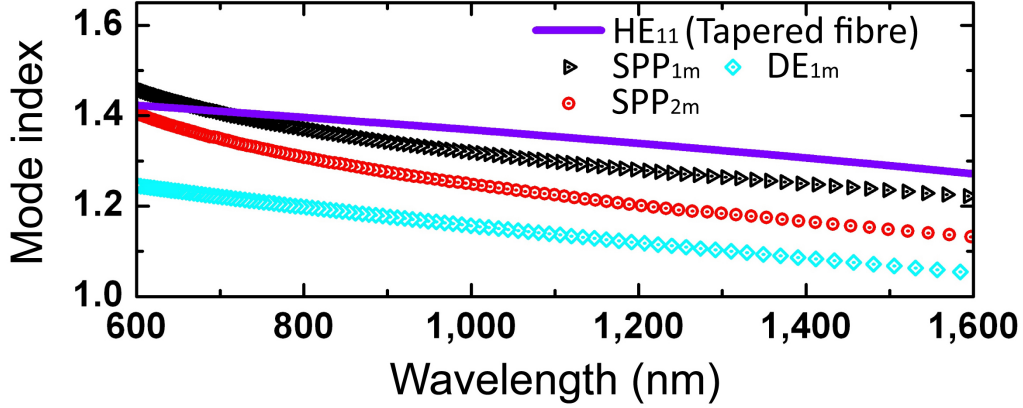


Figure 5.6. Effective cavity mode indices, n_c , of SPP_{1m} , SPP_{2m} and DE_{1m} (with respect to R_b), shown as a function of resonance wavelength. The mode index of a tapered-fiber HE_{11} mode is shown to demonstrate phase matching.

5.4.1 Fiber and SPP resonator phase matching

The cavity mode index, n_c , of a specific eigenmode can be evaluated with respect to the dielectric cavity edge ($r = R_b$) as $n_c = mc/2\pi R_b f$. Figure 5.6 shows the calculated mode index for modes SPP_{1m} , SPP_{2m} , and DE_{1m} . The mode index of a fundamental surface-plasmonic mode (SPP_{1m}) is larger than that of a fundamental dielectric mode (DE_{1m}) within most of the visible and near-infrared frequency band, due to the plasmonic surface-wave characteristics. The mode index is important because it determines the phase matching condition for excitation of SPP modes by a tapered fiber.

After n_c has been calculated, the corresponding phase matched fiber mode index can be obtained by two different approaches. (1) Using the coupled-mode theory, the evaluation of the coupling coefficient κ involves the overlap integral of the cavity eigenmode and the tapered-fiber eigenmode. To have a non-zero coupling strength, the waveguide mode index can be approximated by setting the ϕ dependence of the integrand to zero to give

$$n_w \approx n_c \frac{\sin^{-1} \sqrt{\delta(2-\delta)}}{\sqrt{\delta(2-\delta)}} = n_c \left(1 + \frac{1}{3}\delta + \frac{2}{15}\delta^2 + O(\delta^3)\right) \quad (5.1)$$

where $d = -d_g/R_b \geq 0$ denotes the relative gap width (d_g , gap width).

(2) Alternatively, the phase-matching condition can be found by path-averaging the effective mode index seen by the straight fiber waveguide [96]. This gives exactly the same formula

$$n_w \approx n_c \frac{2 \tan^{-1}(\delta/\sqrt{\delta(2-\delta)})}{\sqrt{\delta(2-\delta)}} = n_c \left(1 + \frac{1}{3}\delta + \frac{2}{15}\delta^2 + O(\delta^3)\right) \quad (5.2)$$

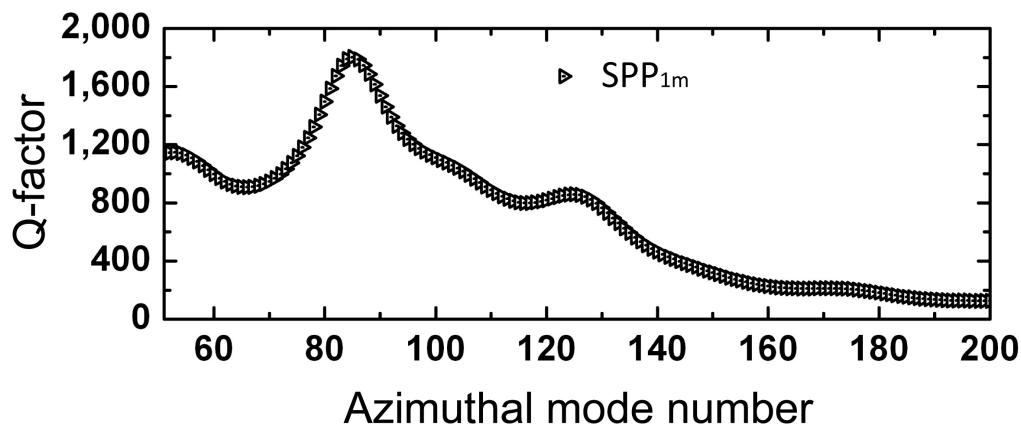


Figure 5.7. The theoretical Q factor for SPP_{1m} , plotted as a function of azimuthal mode number, m

confirming the asymptotic dependence of phase matching on the relative gap width, δ . This formula applies only to the case of negative gap width, that is, $\delta = -d/R_b \geq 0$.

To qualitatively describe the effect of gap width variation on the phase matching, the HE_{11} mode index of a fiber waveguide with a $1\text{-}\mu\text{m}$ waist diameter is shown in Figure 5.6. The fiber mode index is slightly larger than the SPP_{1m} mode index in the near-infrared wavelength band. However, owing to the above phase-matching formula, the SPP_{1m} eigenmode can be effectively phase-matched to the tapered-fiber eigenmode by increasing the relative gap width. The diameter of the tapered fiber can be optimized to phase-match the cavity eigenmodes to the fiber eigenmode.

5.4.2 SPP resonator quality factor

The calculated cavity Q factors for SPP_{1m} eigenmodes as a function of azimuthal mode number, m , are presented in Figure 5.7. The calculated Q factors consist of contributions from intrinsic metal loss (silica material loss is negligible in comparison with metal loss [11, 94, 95]) and the geometry- and material- dependent radiation loss into free space: $Q^{-1} \approx Q_{metal}^{-1} + Q_{rad}^{-1}$. Therefore, this Q value provides the ideal theoretical limit on the Q performance of SPP microdisk resonators that have negligible scattering loss induced by surface roughness.

From the finite-element eigenfrequency analysis, the complex-valued eigenfrequency, $f = f_{re} + if_{im}$, can be calculated, and Q factors evaluated using the formula $Q = f_{re}/2f_{im}$. The radiation-limited Q factor can be estimated and separated from the metal-loss-limited Q factor by removing the imaginary part of the permittivity of silver. For example, the radiation-limited Q factor for $m = 54$ (Figure 5.7) is 3.9×10^6 , and for $m = 85$ the Q factor is 6.7×10^9 , both of which are orders of magnitude larger than the total Q factors.

The radiation-limited Q factor, Q_{rad} , is orders of magnitude larger than the metal-loss-limited Q

factor, Q_{metal} ; the ideal SPP microcavity is thus metal-loss limited: $Q^{-1} \approx Q_{metal}^{-1}$. In Figure 5.8a, the highest fundamental SPP Q factor is found to be 1,800 at the resonant wavelength of 1,062.45 μm ($m = 85$). At a wavelength of 1,568.25 μm ($m = 54$), which is close to the value used in measurements described below (Figure 5.8a), the theoretical Q factor is 1,140.

5.5 Plasmonic resonator results

5.5.1 Testing setup

To measure the SPP microdisk resonances experimentally, a narrow linewidth (< 300 kHz) tunable external-cavity semiconductor laser is coupled to the tapered fiber waveguide and scanned over the 1,520–1,570 nm wavelength range. The position of the tapered fiber with respect to the SPP microdisk resonator is controlled at a fixed vertical distance by piezoelectric stages with 100 nm resolution, and the laser polarization is controlled using a fiber polarization controller and monitored with a polarimeter. For large overlap between the cavity and the waveguide modes, the tapered fiber is positioned underneath the bevelled edge of the resonator, where the silica microdisk is free of silver coating. The output transmission is recorded using a photodetector and a digital oscilloscope.

5.5.2 Measured quality factors

Figure 5.8a shows the normalized transmission spectrum from an SPP microdisk resonator with a Lorentzian line-shape fit (Figure 5.8a, red curve) to each resonance. Two resonances, located at 1,523.59 and 1,532.76 nm (SPP_{1,83} and DE_{1,74}, as estimated by calculation), can be clearly identified. An expanded view of the scan (main panel modes outlined) is shown in the inset of Figure 5.8a and spans three free spectral ranges of SPP and dielectric eigenmodes. The cavity Q factor for the fundamental SPP_{1,83} eigenmode is found to be 1,377 (which falls within the theoretical Q -factor range of $760 \leq Q \leq 2,360$, with a nominal Q factor of 1,225 for the SPP_{1,83} eigenmode), and that of the fundamental DE_{1,74} mode is 4,025. This SPP Q factor of 1,376 is over 30 times larger than the Q factors reported in previous SPP cavity work [97, 27, 98, 99, 100], and larger than the Q factor measured in the gold coated microtoroid the author studied.

To determine the reproducibility of this Q factor, two series of samples of different nominal sizes (series 1, $R_b = 10.93 \mu m$; series 2, $R_b = 15.56 \mu m$) were tested. The measured Q factors for both the SPP and dielectric eigenmodes in the 1,550 nm wavelength band are plotted statistically in Figure 5.8b. Two separate clusters of Q factors are seen in this plot, indicating the distinctive resonant characteristics of the two sorts of eigenmode and a tendency for loss to decrease (Q factor to increase) as the size of the cavity increases.

To test the metal-dependent resonance characteristics of the SPP microdisk, chromium (which is

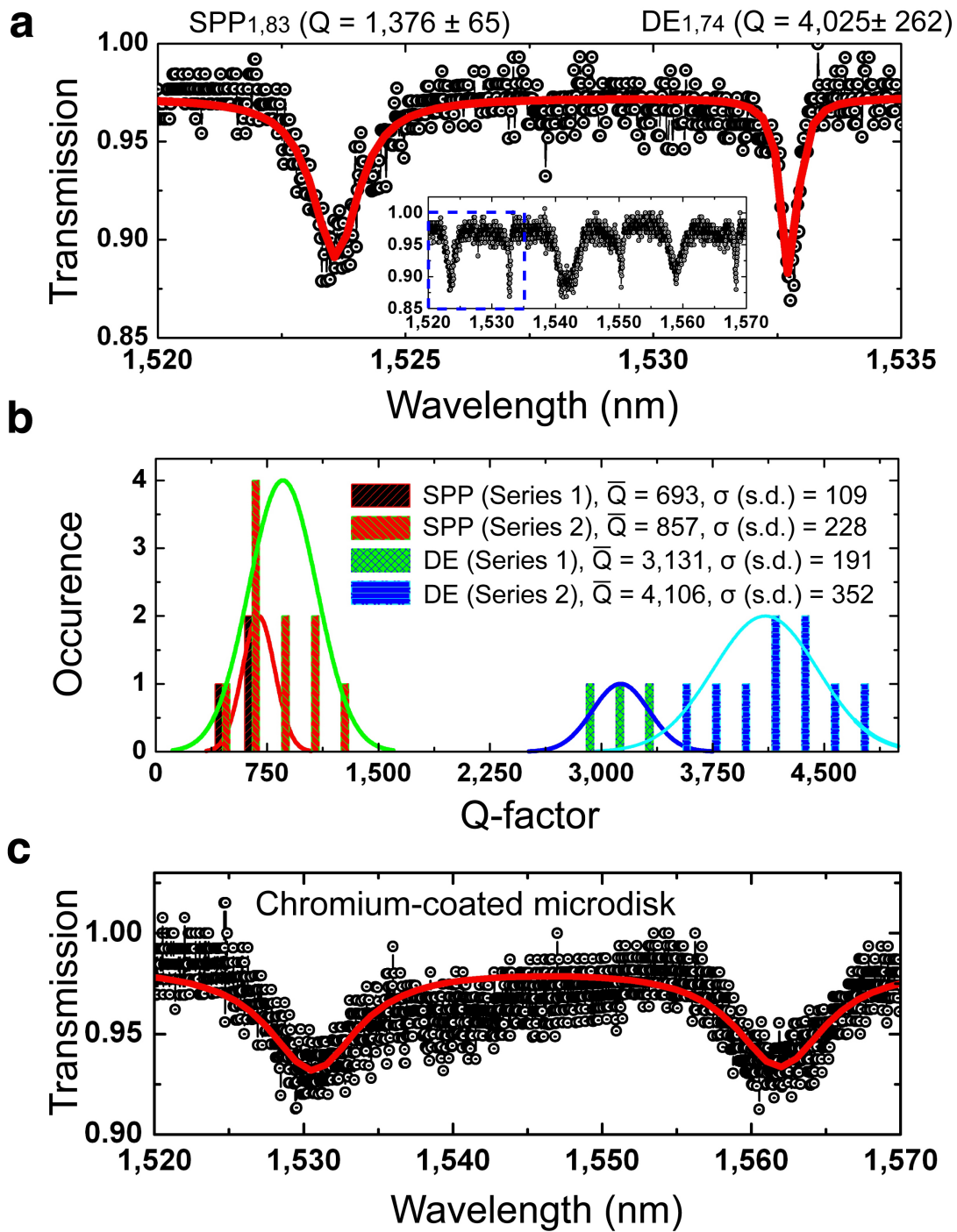


Figure 5.8. **a**, Normalized transmission spectrum showing the highest measured SPP Q factor of 1,377 and a dielectric resonance with a Q factor of 4,025. **b**, Statistical histogram of measured Q values for two different sample batches (series 1 and series 2). Mean (\bar{Q}), and standard deviation (σ) of Q factors are shown in the key (series 1, $n = 3$ measurements; series 2, $n = 9$). **c**, Normalized transmission spectrum for a chromium-coated microdisk resonator with Lorentzian fit

highly lossy at optical frequencies) was deposited onto the silica microdisk using the same sputtering process, for use in control experiments. The normalized transmission spectrum for a chromium-coated microdisk resonator is shown in Figure 5.8c. In this case, only low- Q resonances (for example $Q \approx 213$ at 1,561 nm) are observed, owing to the presence of the chromium layer. These resonances are primarily of optical dielectric origin, as confirmed by finite-element simulations, because the fundamental SPP eigenmodes of a chromium-coated microdisk of this size should have a theoretical Q factor of ~ 10 in the 1,550 nm band.

5.5.3 SPP modes dependence on coupling

To verify the phase-matched excitation of the cavity eigenmodes, a series of measurements were performed with variations in the position of the tapered fiber waveguide relative to the SPP cavity. Figure 5.9 shows the normalized transmission spectra (for an SPP microdisk from a batch from series 2) excited at different gap widths, d_g , and also the corresponding optical micrographs and relative positions between the cavity and the tapered fiber waveguide. Each of the eigenmodes is assigned a mode number (Figure 5.9a) inferred from finite-element simulations. To assign mode numbers to the experimentally obtained resonance spectra, such as those shown in Figure 5.9a, the size of the cavity is measured with a scanning electron microscope and the measured geometrical dimension is used in the finite-element calculation. Owing to the high sensitivity of the resonance frequency with respect to the nanoscale geometrical variation and the permittivity of the component materials, only the approximate mode numbers can be inferred. There being distinct ranges of Q factors indirectly confirms the theoretical SPP and dielectric resonance locations. Then the transmission of each resonance is experimentally determined by varying the gap width and the input polarization to assign distinct resonant characteristics precisely to each of the eigenmodes.

The importance of the phase matching between cavity and fiber eigenmodes is manifest in the observed transmission spectra. At larger gap widths ($d_g \approx 0.8, 0.4 \mu\text{m}$), only the resonances of the first and second-order SPP eigenmodes (SPP $_{1m}$ and SPP $_{2m}$) are observable, and the fundamental dielectric eigenmode (DE $_{1m}$) resonances are absent. This is because, for this range of larger gap widths, SPP eigenmodes are better phase-matched to the fiber eigenmode [96] and have a larger field overlap with the fundamental fiber eigenmode (they are located closer to the edge of, and extend farther outside, the microcavity than does the fundamental dielectric eigenmode in the wedge-shaped structure). As the gap width decreases further ($d_g \leq 0$), the fundamental dielectric eigenmodes are excited, as the phase-matching condition can be partly satisfied by decreasing d_g . For negative gap width, the SPP resonances are even more pronounced, as the phasematching condition between the SPP and fiber eigenmodes can be fully satisfied owing to gap-width-induced phase matching, as is shown qualitatively in Figure 5.6. For the SPP resonance at 1565.4 nm, an input power transfer of up to 50% is demonstrated, showing the effectiveness of phase-matching control using the tapered

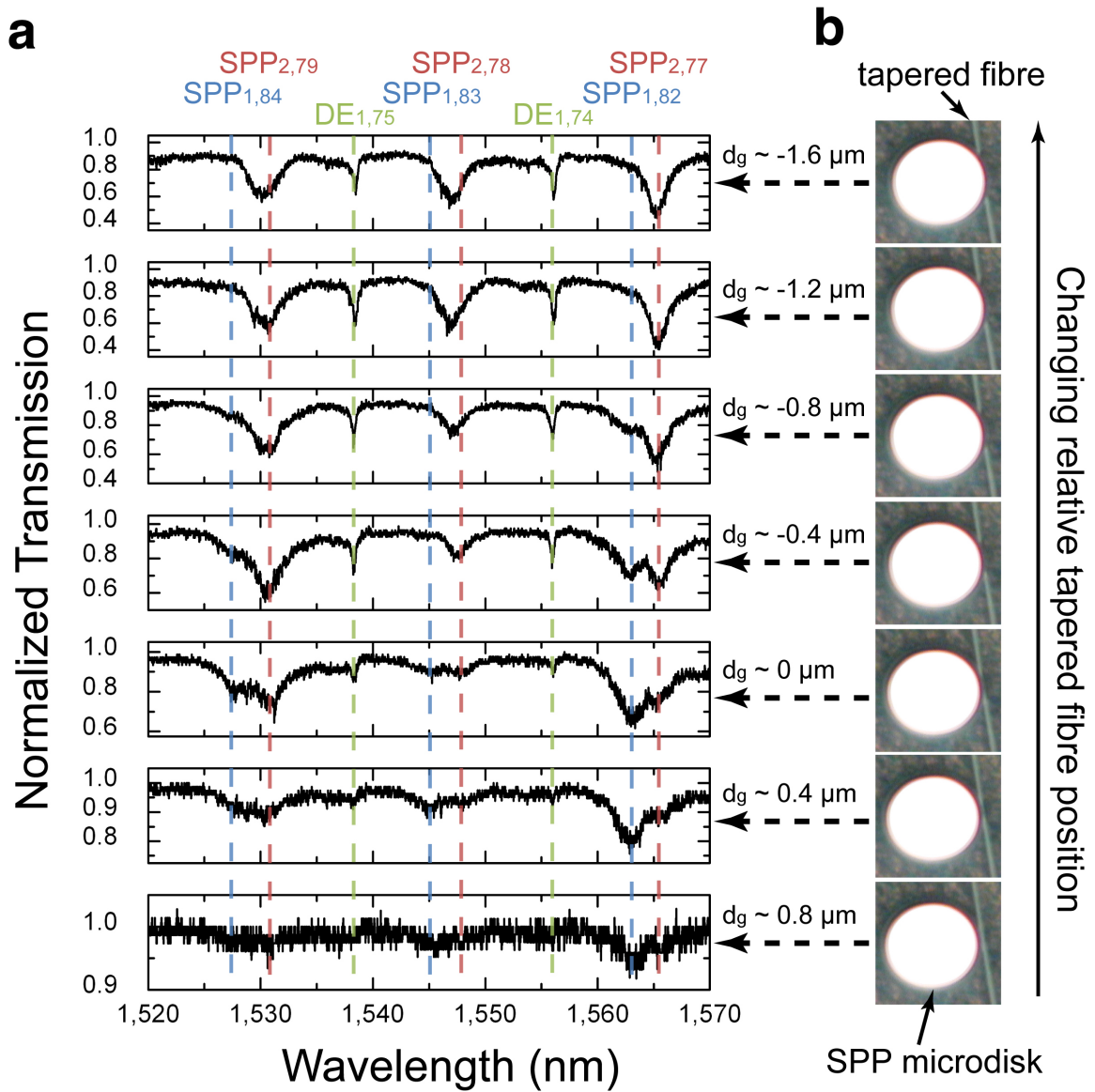


Figure 5.9. Transmission spectrum versus waveguide coupling gap. **a**, Series of normalized transmission spectra, recorded for a variety of gap widths between the tapered fiber waveguide and the edge of the SPP microdisk. Resonances of SPP and dielectric eigenmodes are shown with estimated mode numbers. $R_b = 15.71 \mu\text{m}$, $R_t = 13.09 \mu\text{m}$, $d = 2 \mu\text{m}$, $t < 100 \text{ nm}$. For the SPP resonance at 1565.4 nm , an input power transfer of up to 50% is demonstrated (second panel from the top). **b**, Optical micrographs corresponding to the recorded normalized transmission spectra. Estimated gap width, d_g , is also shown.

fiber waveguide.

5.6 Application of SPP resonator

The demonstration of high- Q surface-plasmonic microcavities opens many possibilities for applications in fields ranging from fundamental science to device engineering. As a specific example, it could make possible a plasmonic laser, for which adequate gain materials as well as a high- Q SPP cavity are key prerequisites [101]. Although the demonstrated SPP Q factor is still less than that of an optical micro- or nanocavity [78, 102], the corresponding SPP loss coefficient of $\alpha_{\text{SPP}} \approx 2\pi n_c / \lambda Q_{\text{SPP}} \approx 39 \text{ cm}^{-1}$ (where λ is the wavelength) satisfies the experimental criteria for a laser cavity and shows that, in principle, such surface-plasmonic lasing devices are possible. The tapered-fiber excitation scheme also demonstrates a convenient means of exciting these structures and selectively probing SPP cavity modes, because it directly controls the mode overlap and phase matching between the cavity and fiber eigenmodes. Furthermore, it is notable that the SPP Q factor could be substantially increased beyond the values measured here by lowering the temperature of the SPP microcavity [101, 103]. From a fundamental standpoint, the SPP Q factor is sufficient to observe interesting cavity quantum electrodynamical phenomena in the weak-coupling regime relating to enhanced Purcell factors [102, 104, 105]. In addition, using the high nonlinearity of metal (or materials deposited in the vicinity of the metal), it may be possible to extend the applications of nonlinear plasmonics. Finally, it should be noted that, because the $\lambda^3 Q/V$ values of the present SPP microcavity (approximately a few hundred) are still much less than those provided by the photonic-crystal and dielectric whispering-gallery microcavities [78, 102], it is still important to pursue new plasmonic cavity designs.

5.7 Summary

Surface plasmon polaritons (SPPs) are electron density waves excited at the interfaces between metals and dielectric materials [106]. Owing to their highly localized electromagnetic fields, they may be used for the transport and manipulation of photons on subwavelength scales [24, 25, 87, 26, 88, 89, 90, 91]. In particular, plasmonic resonant cavities represent an application that could exploit this field compression to create ultra-small-mode-volume devices. A key figure of merit in this regard is the ratio of cavity quality factor, Q (related to the dissipation rate of photons confined to the cavity), to cavity mode volume, V [78, 102]. However, plasmonic cavity Q factors have so far been limited to values less than 100 both for visible and near-infrared wavelengths [97, 27, 98, 99, 100]. Significantly, such values are far below the theoretically achievable Q factors for plasmonic resonant structures. In this chapter, a high- Q SPP whispering-gallery microcavity was presented, made by

coating the surface of a high- Q silica microresonator with a thin layer of a noble metal. Using this structure, a maximum Q of 1,377 was achieved in the near infrared for surface-plasmonic whispering-gallery modes at room temperature. This nearly ideal value, which is close to the theoretical metal-loss-limited Q factor, is attributed to the suppression and minimization of radiation and scattering losses that are made possible by the geometrical structure and the fabrication method.